

VISIBLE AND NEAR-INFRARED OBSERVATIONS OF THE AEROSOL DEBRIS FROM THE COLLISION OF SL-9 WITH JUPITER: A REVIEW FROM LA PALMA AND CALAR ALTO IMAGING AND SPECTROSCOPY¹

F. Moreno, A. Molina, O. Muñoz, J.L. Ortiz, J.J. López-Moreno
Instituto de Astrofísica de Andalucía, CSIC, PO Box 3004, Granada, Spain

S.M. Larson

Lunar and Planetary Laboratory, University of Arizona, USA

H. Campins

Department of Astronomy, University of Florida, USA

T.M. Herbst, K. Birkle

Max Planck Institut für Astronomie, Heidelberg, Germany

H. Bönhardt

Universitaets-Sternwarte, München, Germany

D. Hamilton

Max Planck Institute für Kernphysik, Heidelberg, Germany

Summary: We present results from analysis of imagery and spectra of the effects of the collision of fragment H of comet Shoemaker-Levy 9 with the Jovian atmosphere. The images were obtained using several narrow-band filters at UV through 2.3 μm wavelength under excellent seeing conditions. The large range in incidence and emission angles at which the impact site was recorded allowed us to obtain the physical properties of the debris particles generated. We found that the particles were confined between 1 and 450 mbar, had a modal radius of 0.15 μm , and an imaginary refractive index of 0.02 in the UV and 0.006 in the 1 μm region, in close agreement with the reported values by West et al. [1995] from Hubble Space Telescope imagery. The derived lower limit of the impactor size correspond to the volume of a sphere of 230 m in diameter.

Introduction

The impact of comet Shoemaker-Levy 9 has been the first collision between two bodies in the Solar System predicted in advance. As such, virtually all the major observatories in the world, both ground-based and spacecraft, devoted a substantial amount of the available time to the observation of the event. We focused mainly on the observation of the impact scars and their temporal evolution. In this paper, we analyzed the aerosol component of the dense core region generated by the impact of fragment H, which was recorded with visible and near-infrared images and spectra under excellent seeing conditions.

¹Based on observations at the 4.2-m William Herschel Telescope at the Roque de los Muchachos and the 3.5-m Telescope at Calar Alto Observatories

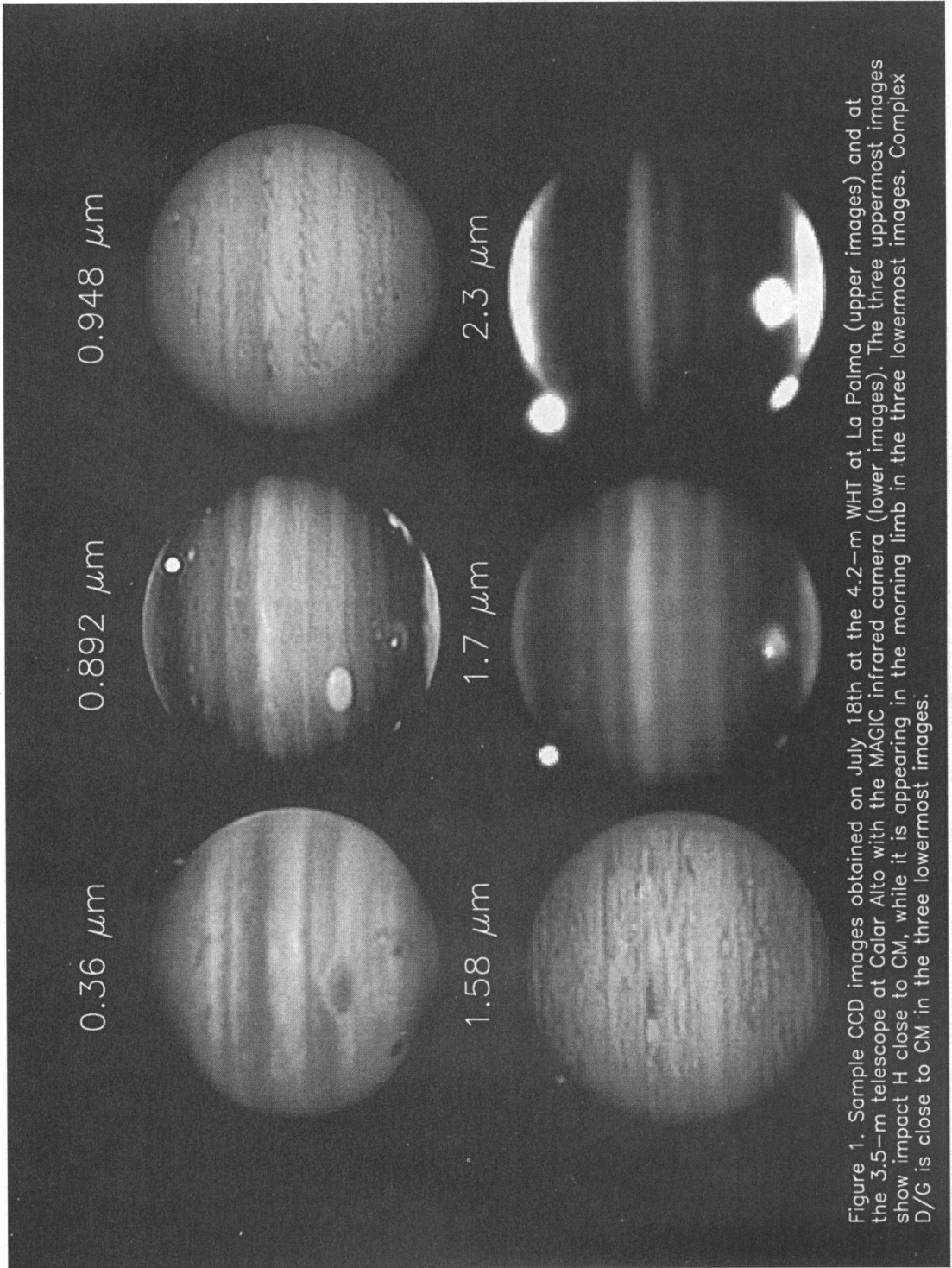


Figure 1. Sample CCD images obtained on July 18th at the 4.2-m WHT at La Palma (upper images) and at the 3.5-m telescope at Calar Alto with the MAGIC infrared camera (lower images). The three uppermost images show impact H close to CM, while it is appearing in the morning limb in the three lowermost images. Complex D/G is close to CM in the three lowermost images.

Observations and data reduction

The present analysis of the H-impact site is focused on CCD images obtained at the 4.2-m William Herschel Telescope at the Observatorio Roque de los Muchachos in the island of La Palma and near infrared imagery and spectra obtained at the 3.5-m Telescope at Calar Alto Observatory in the south of Spain. The CCD images had a spatial scale of 0.102 arcsec/pixel and were obtained through a standard UV filter (effective wavelength 3600 Å) and two narrow-band interference filters at 8920 and 9480 Å with FWHM=50 Å. These narrow-band filters are centered in a strong absorption methane band and its nearby continuum, respectively. We observed the H site at a variety of observational geometries, from the limb to the central meridian, which permits an accurate determination of the limb darkening curve. The observations at the 3.5-m telescope at Calar Alto were made using the near infrared detector MAGIC (Max Planck General purpose Infrared Camera), which is a 256×256 HgCdTe array. We employed four filters centered at 1.5, 1.58, 1.7, and 2.3 μm, with bandpasses of 0.05, 0.01, 0.05, and 0.2 μm, respectively. Spectra of the H site were recorded at both the H and K photometric bands with a resolving power of 360. The image scale was 0.322 arcsec/pixel.

After performing the basic reductions (background subtraction and flatfielding), all the images were geometrically reduced to generate, at each wavelength, a table of μ_0 (cosine of incidence solar angle), μ (cosine of emission angle), $\Delta\phi$ (azimuthal difference between Sun and Earth), and I/F (reflectivity). For the CCD images, the true reflectivities were obtained by considering the geometric albedo determinations by Karkoschka [1994]. The near infrared images and spectra were calibrated by using observations of 16CygB and BS 5868 at airmass close to that of Jupiter. These calibrations were further checked by the use of galilean satellites (see Moreno et al. [1995] and Ortiz et al. [1995] for details). A sample of the images obtained is given in figure 1.

The methane absorption coefficients in the 8920 and 9480 Å filter bandpasses were obtained from Giver [1978]. The near infrared spectrum was modeled by considering the exponential-sum fits to narrow-band laboratory transmission data of methane (for details, see Ortiz et al., [1995], and Baines et al. [1993]). H₂-H₂ and H₂-He collision-induced absorption, which affect the computed reflectivities near 2.1 μm, was also included in the models by using FORTRAN codes kindly sent by A. Borysow (see Borysow, [1991]; Borysow, [1992]).

Model results and conclusions

Once generated the above mentioned tables, we started the analysis of the atmospheric aerosol structure by using a Mie code in combination with a discrete-ordinates radiative transfer code called DISORT (Stamnes et al., [1988]). Given the high reflectivity of the impact sites at the deep absorption methane bands, we assume that the aerosols are distributed above the ammonia cloud. The persistence of the debris cloud is also indicative of a small size of the aerosols, which we assume to be less than 0.5 μm in radius. With these two constraints, we solved for the best fitted imaginary refractive index as a function of wavelength, the par-

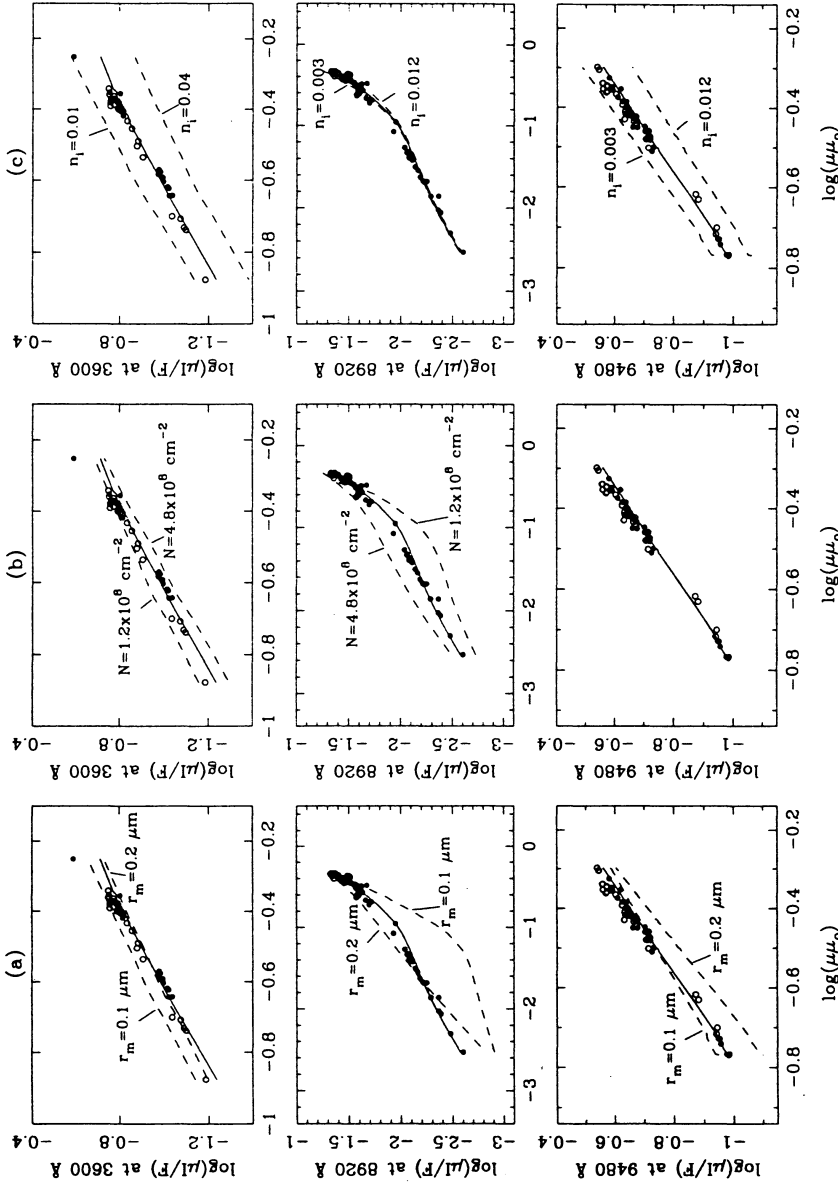


Figure 2.- (a) The limb darkening dependence of the aerosol debris in the core of the impact H region, at three wavelengths, 3600, 8920, and 9480 Å. The solid circles are the data points corresponding to July 18th, 1994, and the open circles those corresponding to July 21st. The solid line is the best model fit, corresponding to a particle size of $0.15 \mu\text{m}$ in modal radius. The upper layer of the model is located at pressure levels between 1 and 350 mbar, with a column density of particles of $2.4 \times 10^8 \text{ cm}^{-2}$. The lower layer is located between 350 and 450 mbar and has a column density of $8 \times 10^9 \text{ cm}^{-2}$ particles. The best-fitted imaginary refractive indexes were 0.02 at 3600 Å and 0.006 in the near infrared. The dashed lines show the model results when the particle radii are varied as indicated. (b) as (a), but including, in dashed lines, the results of the model computations for different particle column densities in the 1–350 mbar range. (c) as (a), but including, in dashed lines, the results of the model computation for different particle imaginary refractive indexes.

title radius (which was assumed also to be constant with height), and the column concentration of particles in a multilayered atmosphere above the NH_3 cloud. We assumed a log-normal size distribution for the particles with $\sigma=1.2$ (the width of the distribution). The real refractive index was another fixed parameter in the models, which was set to 1.7. For the base cloud of the models, we assumed a semi-infinite cloud characterized with a two-term Henyey-Greenstein phase function with parameters $g_1=0.8$, $g_2=-0.8$, and $f_1=0.969$, and single scattering albedo of 0.997.

With all of the above assumptions, we find that the best fitted parameters satisfying both the “visible” and near infrared imagery and spectra are those specified in table 1. Figure 2 shows the quality of the fits to the CCD imagery data, and the sensitivity of the model parameters involved to the model results. Figure 3 shows the same but for the near infrared spectra at the H and K bands. In the assumption that all the debris material we see is coming from the impacting body, and considering the area of the impact site, a lower limit to the impactor’s size would be that of a sphere of 230 m in diameter.

Table 1.- Nominal model parameters for the H impact site.

n_i (3600 Å)	n_i (9000 Å)	n_i (1.6–2.5 μm)	r_m	N (1–350 mbar)	N (350–450 mbar)
0.02	0.006	10^{-4} – 10^{-3}	0.15 μm	$2.4 \times 10^8 \text{ cm}^{-2}$	$8.0 \times 10^9 \text{ cm}^{-2}$

From the models, it is retrieved a considerable amount of aerosols in the stratosphere, although the largest component would be placed at the 350–450 mbar range. This would be consistent with the fact that the aerosols are observed to have a motion consistent with the dominant zonal wind profile at these latitudes (Hammel et al., [1995]). In that respect, we observed a zonal motion for the K complex debris clouds of 7 m/s eastward (in System III) from images obtained on July 22 and August 10th (Moreno et al., [1994]).

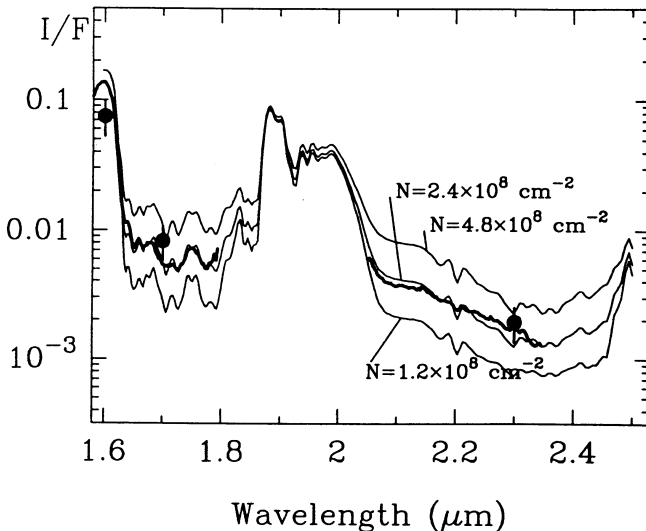


Figure 3.- Near infrared spectra at the H impact site obtained with the MAGIC camera at the 3.5-m telescope at Calar Alto (thick lines). The thin lines represent the model calculations for the nominal model parameters of table 1, except for a higher ($8 \times 10^{11} \text{ cm}^{-2}$) column concentration of particles in the 350–450 mbar region. Results are shown for three different particle column concentration in the 1–350 mbar range. All the features observed are due to methane absorption except at 2.1 μm region, in which the spectrum is dominated by H_2 – H_2 collision-induced absorption. The filled circles represent the data from the imagery obtained at the same observational geometry.

Our models also set a constraint on the composition of the aerosol material through the reported values of the imaginary index. These values are in accordance with those reported by West et al. [1995] from a global analysis of all the impact sites. West et al. [1995] conclude that the color of the material may be due to an organic material rich in nitrogen and sulfur. However, a more precise knowledge of the nature of the aerosol material would be needed to understand the physical processes involved during the fireball phase. Also, models of the long-term evolution of the aerosols and their motion in the stratosphere would be needed to understand the stratospheric dynamics.

REFERENCES

- Baines, K.H., R.A. West, L.P. Giver and F. Moreno. *J. Geophys. Res.*, *98*, 5517, 1993.
- Borysow, A. *Icarus*, *92*, 273, 1991.
- Borysow, A. *Icarus*, *96*, 169, 1992.
- Giver, L.P. *J. Quant. Spectros. Rad. Transfer*, *19*, 311, 1978.
- Hammel H.B. et al., *Science*, in press, 1995.
- Karkoschka, E. *Icarus*, *111*, 174, 1994.
- Moreno et al. *Bull. Amer. Astron. Soc.*, *26*, 1059, 1994.
- Moreno et al. *Geophys. Res. Lett.*, in press, 1995.
- Ortiz et al. *Geophys. Res. Lett.*, in press, 1995.
- Stamnes, K., Tsay, S.C., Wiscombe, W., and Jayaweera, K. *Appl. Optics*, *27*, 2502, 1988.
- West, R.A., et al. *Science*, in press, 1995.

ACKNOWLEDGEMENTS

The 4.2-m William Herschel Telescope is operated on the island of La Palma by the Royal Greenwich Observatory in the Spanish Observatorio del Roque de los Muchachos of the Instituto de Astrofísica de Canarias. The staff of the William Herschel Telescope at La Palma is particularly acknowledged, specially the very kind assistance of Renée Rutten. Thanks also go to Rafael Rebolo and K.C. Sahu for their support and patience during our observations.

The data presented here were partially obtained with the 3.5-m telescope of the Calar Alto Observatory in Spain. We are grateful to Ulrich Thiele, Andrea Richichi, Giovanni Calamai, Carl-Heinz Mantel and Alex Fiedler, who formed part of the SL-9 Calar Alto Observing Team together with some of the authors (Kurt Birkle, Tom Herbst, Doug Hamilton, Hermann Böhnhardt and Jose Luis Ortiz). Robert A. West generated software for the quasi-random band modelling and the exponential sum fitting of the methane laboratory data. A. Borysow kindly sent the FORTRAN codes for the computation of the H₂-H₂ and H₂-He collision-induced absorption.

This research was supported by the Comisión Nacional de Ciencia y Tecnología under contracts ESP94-0719, ESP94-0803, and ESP93-0338.